*Manuscript
Click here to view linked References

ON THE UNDERESTIMATED EFFECT OF THE STARCH ASH ON THE CHARACTERISTICS OF LOW COST CERAMIC MEMBRANES

M-M. Lorente-Ayza[a *], S. Mestre[a,b], V. Sanz[a,b], E. Sánchez[a,b]

[a]Instituto Universitario de Tecnología Cerámica. Universitat Jaume I. Castellón. España

[b]Departamento de Ingeniería Química. Universitat Jaume I. Castellón. España

***Corresponding Author**: M-Magdalena Lorente-Ayza

Phone: +34 964 34 24 24

Fax: +34 964 34 24 25

E-mail: *magda.lorente@itc.uji.es*

Postal address: Instituto de Tecnología Cerámica

Campus Universitario Riu Sec

Av. Vicent Sos Baynat s/n

12006 Castellón (Spain)

Abstract

Starches are commonly used as a pore generator in the fabrication of low-cost ceramic membranes, since they are cheap, innocuous, environmentally friendly and easy to burn. Nevertheless, the influence of starches residues (ashes) generated during its burning off is dismissed. The present study analyses the influence of the starch ashes, generated by six different starches of similar particle size, on the characteristics of low-cost ceramic supports. The results indicated that starches gave rise to different amounts of ashes ranging from 0.17 to 0.71 wt%. In addition, these ashes contained some chemical

elements in their composition, such as sodium, potassium or calcium, which can act as fluxes in the ceramic composition, modifying the characteristics of the obtained supports (mainly open porosity, water permeability and pore size distribution). It has also been observed that when the ash content grows the effect of the fluxing elements on the evolution of the microstructural features of the ceramic membrane (porosity, pore size or permeability) becomes more significant. Finally, tortuosity was calculated with a simple model derived from the Hagen-Poiseuille equation; the obtained data showed that tortuosity factor and its evolution with dwelling time were also affected by the starch ashes.

Keywords: B: Porosity; E: Membrane; Starch; Permeability; Tortuosity

1 Introduction

Processes based on membranes are widespread in the industry because of their numerous applications for the treatment and purification of wastewater. The two most common membranes are polymeric and ceramic. For the ease of manufacturing and lower cost, polymeric membranes find much more industrial applications [1]. However, ceramic membranes exhibit interesting advantages over the polymeric ones such as their greater resistance to temperature and chemical attack as well as reduced tendency to fouling [1–6].

Ceramic membranes traditionally consist of a multilayer assembly of a ceramic support and one or more selective layers, adopting different configurations, discs, plates, tubes, fibres, etc. The materials used have essentially been refractory ceramic oxides such as alumina, zirconia or titania, due to their excellent chemical resistance. As manufacturing processes, the support is typically shaped by extrusion or powder consolidation whereas

the selective layers are deposited on the support by conventional application techniques such as spraying or dipping or more sophisticated techniques such as sol-gel [1–4,7]. However, for many applications of ceramic membranes, high-purity refractory oxides are not necessary as a raw material. Such is the case, for example, of industrial or domestic wastewater treatments in which the quality requirements of treated effluent can be achieved with ceramic membranes obtained with more conventional materials. This would imply a significant reduction of the ceramic membrane cost associated with a lower cost of raw materials and manufacturing process.

As a result of the above, in recent years there has been a growing interest in the scientific community for research into conventional ceramic raw materials which allow to design cheaper ceramic compositions. These new compositions can be used for the manufacture of low-cost ceramic membranes. Thus many raw materials, additives and even wastes have been tested at a laboratory and pilot scale to be incorporated in this type of membrane compositions [8–18].

One of the essential ingredients in such compositions is the pore former. It is a substance of organic nature with a known particle size that, after being burnt out during the sintering thermal treatment, gives rise to a connected pore network which significantly contributes to enhance membrane permeability. In theory, almost any organic material that burns away during heating can be used as pore former. Thus numerous materials have been reported to impart macroporosity to ceramic bodies such as chemically pure substances (urea [19]), processed substances (starch [20–28] or flour [29]), natural products (poppy seeds [30]) or even wastes (sawdust or fly ash [8,16,31,32]). Starch is one of the most frequently used pore-forming agents due to its chemical composition (a polysaccharide consisting theoretically of C, H and O). Hence this natural biopolymer is easy to burn, inexpensive and environmentally friendly

[25,33–37]. However, starch, as a substance derived from natural sources, exhibits a wide range of characteristics that can affect the final properties of the resulting membranes [25,35,36,38]. Generally in each investigation the nature of the starch used is kept fixed, therefore the effect of the starch characteristics on the ceramic body properties hardly has been observed and discussed in the literature [22,24,36,37]. Recently, Lorente-Ayza et al. have shown the significant effect of particle size of the starch on the characteristics of ceramic membranes obtained with conventional raw materials [38]. To conduct their study, the authors employed seven starch samples out of five different sources. These authors demonstrated the key role of particle size of the starch on the porous membrane structure and consequently on its permeability.

On the other hand, most reported papers recognize the low proportion of combustion residue (ash) as one of the main advantages for the use of starch as pore generator. For this reason, the possible effect that the starch ash exerts on the characteristics of the ceramic membrane has not been addressed in the literature. While the ash content of starch generally lies under 1 wt% [38], its effect when a specific porous structure is required should not be underestimated.

For the above reasons it is considered of great interest to address a research aiming at quantifying the possible influence that content and nature of the starch ash may exert on the final characteristics of a ceramic membrane obtained from low cost raw materials. This objective certainly requires the use of different starches that give rise, in turn, to different proportions of ashes of diverse chemical composition. These starches will be added to a standard low cost ceramic membrane composition that will allow to assess the effect of a given ash content on the processing and final characteristics of the ceramic membrane.

2 Experimental

2.1 Raw materials

Six different starches of diverse sources were selected as pore generators. Some details of these starches are summarized in Table 1. These materials were processed as received, in powdery state.

Table 1. Source and provider of the starches used in this work.

Reference	Source	Provider
M1	Corn	Roquette Freres S.A., France
M2	Potato	Sigma-Aldrich Co. USA
M3	Potato	Roquette Freres S.A., France
M4	Wheat	Fisher Chemical, USA
M5	Wheat	Roquette Freres S.A., France
M6	Pea	Roquette Freres S.A., France

The particle size distribution of the as-received starches was obtained with a laser diffraction particle size analyser (Mastersizer 2000, Malvern Instruments Ltd. UK). The water content was measured by drying the starches in an oven at 110ºC until constant weight. The ash content of starches was determined by treating every dried starch at 1000ºC (RHF 1600, Carbolite, UK) for 60 minutes. According to the literature, these conditions assured the total burnout of the starch [25,36,39]. Finally, the chemical analysis of the ashes was performed by EDX (Genesis 7000 SUTW, EDAX, USA), connected to a FEG-SEM (Quanta 200F, FEI Co, USA).

2.2 Membrane synthesis

Three inorganic raw materials were used to prepare low cost ceramic membranes: a Spanish clay mixture, calcite (OMYACARB 5-BE, Omya AG, Spain) and industrial chamotte. All these raw materials are commonly used in the tile manufacturing industry in Spain. The raw materials were dry milled in a ball mill until practically no particles over 60 μm mesh were left. Finally, the six starches were introduced in the compositions as an organic pore former. Table 2 shows the chemical and mineralogical composition of these raw materials. Figure 1 describes the particle size distribution of the three ground inorganic materials obtained with the laser diffraction particle size analyser.

Table 2. Chemical and mineralogical compositions of the raw materials used (wt %).

	Clay mixture	Calcite	Chamotte
SiO_2	67.2	0.24	70.1
Al_2O_3	20.3	0.15	20.4
Fe_2O_3	1.1	0.02	1.7
CaO	0.4	55.7	0.5
MgO	0.5	0.14	0.4
Na_2O	0.2	-	4.3
K_2O	3.0	0.01	2.0
TiO_2	1.0	-	0.7
Loss on ignition	6.3	43.7	-
Mineralogical composition	Kaolinite, Quartz; Albite, Microcline (potassium feldspar) Muscovite, Hematite	Calcite	Quartz, Albite, Microcline, Hematite

From these materials, six compositions were formulated as shown in Table 3, adding the same proportion of every starch to the same base composition (B0). The proportions of the different composition ingredients were fixed from previous experience by the authors with low cost ceramic membranes formulations [23,38,40].

Table 3. Ceramic membrane compositions prepared in this work (wt %).

Composition	B0	B1	B2	B3	B4	B5	B6
Clay	60	40	40	40	40	40	40
Chamotte	20	20	20	20	20	20	20
Calcite	20	20	20	20	20	20	20
M1	-	20	-	-	-	-	-
M2	-	-	20	-	-	-	-
M3	-	-	-	20	-	-	-
M4	-	-	-	-	20	-	-
M5	-	-	-	-	-	20	-
M6	-	-	-	-	-	-	20

The raw materials were homogenised and moistened to a content of 5.5 kg H_2O/100 kg dry solid. Cylindrical test specimens of 50 mm diameter and 7 mm thickness were formed by uniaxial dry pressing at 250 kg·cm^{-2} in a laboratory unidirectional press (Model Mignon, Nannetti, S.r.l., Italy) and dried in an oven at 110ºC. The dry specimens were then sintered in a laboratory electric kiln (Model Rapido, Pirometrol S.L., Spain) with a thermal cycle characterised by a slow firing cycle up to 500ºC (to complete starch burnout) and a soaking time of 6, 60 and 120 minutes at maximum

temperature (1160ºC), as shown in Figure 2. The maximum temperature was chosen from the results of previous research by the authors [40].

The porosity of both dry and sintered membranes was determined by bulk density determination (Archimedes method) [41].

2.3 Sintered membranes characterization

Water uptake was determined as a simple method to calculate open porosity of membranes. Thus water uptake was measured by the boiling water immersion method and open porosity was calculated by means of this value and sintered bulk density [42]. Pore size distribution was measured by mercury intrusion porosimetry (AutoPore IV 9500 Micromeritics, USA) and the average pore size (d_{50}) and characteristic diameters (d_{16} and d_{84}) were calculated [43]. Some sintered specimens were also inspected by electron microscopy (FEG-ESEM Quanta 200F, FEI, USA) on cross-sectional surfaces of the samples. Micrographs were obtained from back-scattered electron mode.

Functionality of the membranes was assessed in terms of water permeability measurements by means of an automatic water permeameter specifically designed for disc configuration samples (LEP101-A, PMI, USA). In this equipment the water pressure applied onto the membrane was varied from 0 to 0.34 bars while the water flow through the membrane disc was automatically determined. From direct application of Darcy's law, permeability constant can be calculated according to the equation 1, where K_p is the water permeability constant (m^2), μ is the water viscosity (0.001 $kg \cdot m^{-1} \cdot s^{-1}$ at 20ºC and 1 atm), E is the membrane thickness (m), slp is the slope of the straight line fit based on Darcy's law ($m^3 \cdot s^{-1} \cdot Pa^{-1}$), and A is the water permeation area (area of chamber section where the membrane is placed, in m^2).

$$\boldsymbol{K_p = \frac{slp \cdot \mu \cdot E}{A}} \qquad \textit{Eq. 1}$$

If the flux values obtained against the applied pressure are represented, a straight line may be obtained and the corresponding slope calculated. When entering the slope value in the equation of Darcy's law, the K_p value determined for the studied membrane is obtained [7,44,45]. Nevertheless, values of water permeability were recalculated in ($L \cdot h^{-1} \cdot m^{-2} \cdot bar^{-1}$) units for better comparison with commercial membrane data [40,46].

3 Results and discussion

3.1 Starch characterisation

The characteristic diameters D_{10}, D_{50}, D_{90} were calculated from the particle size distribution (PSD) obtained by laser diffraction. The parameters D_{90}, D_{50} and D_{10} denote the cut off particle size below which 90%, 50% and 10% of the total particle volume lies respectively. Figure 3 and Table 4 describe the starches' particle size characterization. A fourth column in Table 4 has been also included with the difference between D_{10}, and D_{90} which denotes, in some extent, PSD wideness.

Table 4. Starches' particle size parameters obtained from particle size distribution curves.

Sample	D_{10} (µm)	D_{50} (µm)	D_{90} (µm)	D_{90} - D_{10} (µm)
M1	9	14	22	13
M2	22	39	67	45
M3	26	46	76	50
M4	9	14	23	14
M5	12	20	31	19
M6	17	24	33	16

As it can be observed significant differences in terms of distribution wideness as well as mean particle size can be found among the starch samples. Thus average particle size

(D_{50}) ranges from 14 (samples M1 and M4) to 46 μm (sample M3) whereas the maximum difference between D_{10} and D_{90} which relates to distribution wideness varies in a similar magnitude from 13 μm (samples M1) to 50 μm (starch M3).

Table 5 shows the water content of the as-received starches and the ash content after their burnout. As a consequence of the high hygroscopicity of starch all the samples contain high amounts of water as set out elsewhere [28,34,38]. With regard to ash proportion, although the value lies below 1 wt% in all the samples, the amount of ash significantly varies in the different starch ranging from lower than 0.2 wt% to higher than 0.7 wt%. Hence independently of the chemical composition of the ash this strong variation is expected to influence on the ceramic membrane processability and/or properties once the starch added into the composition has been burnout.

Table 5. Water content of as-received starch samples and ash content after samples' burnout.

Starch	Water content (%)[1]	Ash content (%)[2]
M1	14.6	0.32
M2	16.8	0.17
M3	22.3	0.71
M4	9.9	0.49
M5	14.7	0.37
M6	14.6	0.29

[1] As received

[2] After thermal treatment

The chemical composition of the ashes in terms of elements measured by EDX is shown in Table 6. As it can be seen very complex chemical compositions comprising 9-10 elements which could belong to many different mineralogical constituents [38,47,48]

are observed in the samples. Phosphorous followed by alkaline (potassium and sodium) and alkaline-earth elements (mainly calcium) are the most abundant in the analysed ashes. In this same table, a last row with the total weight amount (referred to the ash content of each starch sample as shown in Table 5) of the most abundant elements with fluxing behaviour in a ceramic process (Na, K and Ca) has been calculated. As it can be seen A2 and A3 ashes provide the lowest and the highest amount respectively of fluxing elements to a hypothetical ceramic composition as a consequence of the lowest and highest value of ash content (0.17 and 0.71 wt% for A2 and A3 samples respectively).

Table 6. Chemical composition in terms of identified elements of the ashes (denoted by A) of the studied starches (wt%). Note that A1 to A6 refers to ashes obtained from M1 to M6 starch samples.

Element (wt%)	A1	A2	A3	A4	A5	A6
Na	10	5.1	0.9	2.2	14	26
Mg	2.5	2.0	1.7	1.1	0.8	1.3
Al	0.3	0.2	-	<0.1	-	0.2
Si	0.9	0.8	0.3	0.4	0.3	0.9
P	24	23	20	20	20	8.3
S	-	-	-	-	-	0.8
K	12	22	6.8	24	7.6	16
Ca	3.2	3.4	14	2.1	4.0	2.1
Cu	2.0	1.4	1.7	1.5	4.1	0.5
Zn	1.6	1.2	1.3	1.1	2.8	0.5
Calculated total amount (wt%) of Na, K and Ca in the ash $[(Na+K+Ca)_A]$ [3]	0.08	0.05	0.16	0.14	0.10	0.13

[3] This amount has been calculated from ash content of Table 5.

3.2 Ceramic compositions processing

Table 7 shows the dry bulk density of the ceramic membranes shaped by uniaxial dry pressing. Except one composition (B1), which exhibits a slightly lower bulk density, the rest of the formed specimens show quite similar bulk density values. Assuming a constant value of true density for all starch samples of 1.51 $kg \cdot m^{-3}$ [38] calculated

porosity of dry specimens ranged from 32 to 34%, while the porosity of composition without starch (B0) is 28%. These high porosity values for the unfired specimens agree with the fact that a high amount of organic substance (starch) in the composition results in an impaired compaction behaviour of the powder during pressing operation as reported elsewhere [20,23,38,49].

Table 7. Bulk density values of unfired support specimens.

Composition	B0	B1	B2	B3	B4	B5	B6
Dry bulk density (g/cm^3)	1.91 ± 0.01	1.52 ± 0.01	1.56 ± 0.01	1.56 ± 0.01	1.54 ± 0.01	1.54 ± 0.01	1.55 ± 0.01

The dry specimens were then sintered following the thermal cycles set out in Figure 2 for three soaking times at maximum temperature: 6, 60 and 120 minutes. Table 8 collects the properties of sintered samples for the six compositions at the intermedium soaking time (60 min): linear shrinkage, water uptake, loss on ignition, sintered bulk density. Overall all the sintering parameters in the different compositions exhibit the expected variation which corresponds to a sintering process with presence of liquid phase as a consequence of the fluxing compound (mainly K_2O) provided by the clay mixture (see Table 2) since the fluxing contribution of the chamotte should be irrelevant due to its inert behaviour at the sintering temperature. However as easily deduced from the table data, the magnitude of the variation experienced by all these parameters with temperature also depends on the nature of the used starch. Taking into account that starch is burnout during the firing step, this variation should be attributable to the fluxing contribution of the starch ash.

Table 8. Sintering parameters of the six ceramic membrane compositions studied at soaking time of 60 minutes (T=1160ºC).

Composition	B0	B1	B2	B3	B4	B5	B6
Linear Shrinkage (%)	0.5±0.1	2.8±0.3	1.6±0.2	1.9±0.1	0.8±0.1	2.8±0.1	2.0±0.1
Water uptake (%)	19.9±0.2	45.2±0.1	46.4±0.6	44.1±0.5	49.4±0.3	43.5±0.2	45.7±0.4
Loss on ignition (%)	13.41±0.02	30.32±0.02	29.78±0.02	29.29±0.02	29.52±0.01	30.17±0.01	30.17±0.02
Sintered bulk density (g/cm^3)	1.72±0.01	1.22±0.02	1.19±0.01	1.22±0.01	1.14±0.01	1.23±0.01	1.20±0.01
Open porosity ε_a (%)	34.2±0.1	55.1±0.2	55.0±0.4	53.8±0.2	56.5±0.2	53.4±0.1	54.6±0.1

Variation of water uptake (a parameter very sensitive to sintering progress) with dwelling time (at firing temperature of 1160ºC, Figure 4), allows to visualise the sintering behaviour of all the compositions with sintering time. Water uptake is an easy-to-determine parameter which represents the open porosity accessible to water. In addition, one further advantage of this parameter deals with the fact that the water content measurement is carried out with the whole fired specimens, what allows to minimise the experimental error in comparison with other methods in which much smaller specimens are used (such as mercury intrusion or image analysis coupled with microscopy inspection). Error bars have been also included in the representation in

order to separate the effect of the microstructure reproducibility (experimental dispersion) in the following analysis. As it can be observed, whereas the initial value of water uptake obtained with the shortest dwelling time (6 min) is quite similar for all the specimens (50-53%), the curves start to diverge from 1 h soaking time. The ceramic pieces exhibit much more different values of water uptake, which ranges from 30 to 45%, for the longest dwell time Besides the curves also show very different profiles since some of them keep a time dependence through the whole time range analysed (from 6 to 120 min) but others exhibit an almost steady variation with time over 60 min of sintering time. In other words: the longer the sintering time the higher the effect of the starch ash on the sintering behaviour of the ceramic membrane compositions.

As also observed in Figure 4 composition B3 (which includes the starch with the highest ash content) shows one of the largest variation in water uptake while composition B2 (which includes the starch with the lowest ash content) exhibits one of the smallest. With an attempt to correlate the sintering behaviour of these two samples, as well as the rest of compositions, Figure 5 has been plotted. This figure tries to relate the variation of water uptake between 6 and 120 min of dwelling time for all the compositions (ΔWU, equation 2) (values directly deduced from Figure 4) against the total amount of fluxing material provided by the different ashes (values of the last row in Table 6, $[(Na+K+Ca)_A]$).

$$\Delta \boldsymbol{WU}(\%) = \frac{\boldsymbol{WU\ 6 - WU\ 120}}{\overline{\boldsymbol{WU}}} \cdot \mathbf{100} \qquad \textit{Eq. 2}$$

Where WU6 is the water uptake at 6 minutes of dwelling time, WU120 is the water uptake at 120 minutes of dwelling time and $\overline{WU}$ is the average value of both dwelling times (6 and 120 minutes).

As it can be seen, except one composition (B1) the rest of samples shows a quadratic relation between the total amount of fluxing elements contained in the starch ash and the

sintering behaviour of ceramic composition in which the starch is added, as a consequence of the fact that similar fluxing elements (Na, K and Ca) are present in the different samples of ash starch. This non-linear relationship (potential law dependence) between sintering progress and the amount of fluxing substance is not surprising since the sintering advancement depends on the amount and viscosity of the liquid phase developed during the thermal cycle, as discussed below. On other hand the reason for the lack of fit for B1 composition could be related in some extent, with the poor pressing compaction of this composition (lower unfired bulk density) as observed in Table 7. Nevertheless, the great variety of chemical elements present in starch´s ashes, as well as the extremely complex mineralogy of the compounds related to these elements, makes it too difficult to establish simple correlations between chemical composition and sintering behaviour. A further research with a reduced number of starch samples of similar nature is now in progress to define these correlations with chemical composition. Nevertheless, Figures 4 and 5 clearly evidence that the effect of the starch ash cannot be underestimated when designing compositions for porous ceramic membranes.

Figure 6 shows the pore size distribution obtained by mercury intrusion for compositions B2 and B3 at the three sintering times: 6, 60 and 120 min. As observed, the curves evidence the progress of the sintering process since as the sintering time increases: i) the curves shift to the right (increasing mean pore size) and ii) the area enclosed by the curves becomes smaller (decreasing porosity). It can also be observed that pore size distribution curves of compositions B2 and B3 confirm the findings observed in Figures 4 and 5, i.e. a low and a high effect of soaking time on the sintering process as a consequence of the lower and higher impact of the ash content on the ceramic composition respectively. As observed this higher sintering sensitivity of

composition B3 gives rise to enhanced pore coarsening as well as porosity decreasing with sintering time when compared with composition B2.

The variation of the mean pore size (d_{50}) of each ceramic membrane with sintering time (Figure 7), confirms that the mean pore size of the ceramic membranes coarsens with time as a consequence of the sintering process, which takes place in the presence of the liquid phase (provided by the alkaline and alkaline-earth oxide content in the starting raw materials). Besides, as set out above, porosity lowers with increasing sintering time [40,50,51]. The evolution with time of the mean pore size depends on the viscosity of the liquid phase during sintering (and, consequently, on the composition and temperature), reaching a value from which it does not change. On the other hand, when dwelling time increases at the same temperature, the sintering process will result in a higher degree of densification, reducing the volume of pores (and porosity) [52,53]. However, the figure also confirms that this evolution is not unique but it depends on the nature of the used starch. Thus, compositions B2 and B3 again show extreme situations in terms of sintering behaviour. Composition B3 (containing starch M3, with the highest ash content) displays the maximum variation of pore size (the highest coarsening effect); whereas composition B2 (containing starch M2, with the lowest ash content) shows quite lower sinterability (coarsening effect), although other composition (for example B1 and B6) exhibit similar variation of pore size. As set out above, with regard to water uptake variation, although the effect of starch's ash content is a key factor affecting the sintering behaviour of the ceramic composition in which the starch is added, the nature of this ash also plays an important role, which can counterbalance to some extent the effect of the amount of ash provided by the starch to the composition during the firing.

Finally, micrographs of some of the sintered membranes were taken by electron microscopy (FEG-ESEM) in back-scattered electron mode. For the sake of simplicity, only the micrographs corresponding to samples which experienced the most significant differences in sintering behaviour (at 6 and 120 min soaking time), as shown in Figure 4, are included in Figure 8. For comparison purposes the micrograph of the standard composition without any starch sintered at the same firing temperature during 60 min is included in this figure (composition B0). These samples are as follows: B2, B3 and B4. Firstly, it can be observed that, independently of the starch used, the addition of 20 wt% starch to the standard low-cost ceramic composition (B0) manages to open and connect the porous microstructure of the composition. This observation coincides with previous research concerning the addition of starch as pore former [23]. In this reported research it is stated that a minimum amount of starch (approximately 10 wt%) is indispensable for obtaining an interconnected porous network in the sintered samples. Secondly, regardless the starch added, all the compositions reveal the progress of the sintering process, as shown by previous microstructural parameters analysis (water uptake and pore size). Hence, as the sintering temperature rises, the mean pore size increases and total (open) porosity decreases. Finally, when the three specimens are compared, it can be observed that differences between the samples starts to be appreciable for the longest sintering times (120 min), as set out by the water uptake and pore size evolution with time. Thus, microstructure of B3 ceramic membrane sintered during 120 min is characterized by lower porosity but larger pores if compared with the equivalent membrane of the B2 composition. An intermediate behaviour is observed with B4 composition as expected.

3.3 Effect on water permeability of the membranes

As set out above, functionality of the membranes was assessed in terms of water permeability measurements by means of an automatic water permeameter. Table 9 presents the water permeability data of the membranes obtained from the six compositions in terms of K_P (m^2) and P_e ($L \cdot h^{-1} \cdot m^{-2} \cdot bar^{-1}$), together with the mean particle size of starch used in each composition.

Table 9. Water permeability of the ceramic membranes obtained from the six compositions together with the mean particle size of the starch used.

Composition	Soaking time (min)	B0	B1	B2	B3	B4	B5	B6
K_p *10^{-14} (m^2)	6	12	100	110	80	70	120	100
	60	31	180	240	250	160	220	200
	120	-	290	250	390	330	290	290
P_e *10^2 ($L \cdot h^{-1} \cdot m^{-2} \cdot bar^{-1}$)	6	62	200	190	130	120	210	180
	60	160	360	450	460	280	420	390
	120	-	570	490	780	690	570	560
D_{50} (μm)	-	-	14	39	46	14	20	24

As it can be observed in the table data, the fired specimens of all the compositions experience a significant increase of permeability with sintering time. This is a direct consequence of the evolution of the fired microstructure, as set out in previous section. Hence, in all the cases, increasing sintering time leads to a less porous microstructure containing larger pores, due to the advance of the sintering process. This can be also

predicted by using simple permeability models such as Hagen-Poiseuille equation, in which the flow through the porous structure depends on the porosity and two power of mean pore size [5]. This dependence of water permeability with microstructure features, which has been extensively reported in the literature, has been also demonstrated with previous low-cost ceramic membranes compositions [23,38,40].

The variation of water permeability with sintering time has been also plotted in Figure 9 to better compare the differences between the six compositions. Again, the errors bars are included in the representation. As observed, the permeability variation of sintered specimens obtained from compositions B2 and B3 follow, in great extent, what it could be expected from their microstructure development with sintering time. Thus, as set out from water uptake and pore size variations with dwelling time (Figures 4 and 6 respectively) permeability evolution of B2 and B3 compositions follow very different tendencies. B3 composition undergoes higher variation, while B2 composition gives rise to a much lower permeability variation with sintering time. For this reason, the differences in water permeability of these two compositions magnify with sintering time, resulting in much larger difference at the longest sintering time (120 min). Hence the water permeability development with sintering time can be explained by means of the microstructure features evolution and is affected in great extent by the ash content of the starch used as pore former. Again, it should be noted that the effect of the ash content is not the only factor affecting the permeability of the membranes, but it certainly plays a significant role.

Although literature does not report the effect of starch ash on the ceramic membrane microstructure and characteristics, the impact of starch particle size on membrane microstructure and permeability has recently been reported. Thus by using 6 different starches of diverse particle size (from 20 to 190 μm of mean particle size) Lorente-Ayza

et al. have shown the effect of starch particle size on the water permeability of the sintered membranes obtained from similar low-cost ceramic membrane compositions [38]. These authors demonstrated that the variation of water permeability with starch particle size follows a potential law, existing a particle size threshold beyond which the permeability dramatically increases. According to these authors, this threshold lies around 50 μm. If we have a look on our starch particle sizes (see Table 4 and Figure 3), we can observe that the particle size of the starches used in this research lies under this threshold. Therefore, it can be stated that the differences in sintering behaviour, as well as in microstructure and permeability of the compositions addressed in this research, are mostly associated with the content and nature of the starch ash.

The Hagen-Poiseuille equation [5] correlates the microstructural properties of membranes (porosity and mean pore size) with permeability by means of the following relation:

$$\boldsymbol{K_p = \frac{e_{sf} \cdot d^2}{32 \cdot \mu \cdot \tau}} \qquad \textit{Eq. 3}$$

where K_p is the permeability coefficient, d the pore diameter, μ the water viscosity, ε_{sf} the surface porosity and τ the tortuosity factor. Assuming that the tortuosity can keep constant in a set of given membranes of similar starting compositions and considering ε_{sf} equals to the open porosity obtained with the water uptake determination (ε_a), the model prognosticates an approximately linear relationship between K_p and $[\varepsilon_a \cdot d^2]$. Figure 10 plots the correlation between water permeability values of all membranes analysed in the study (compositions B1, B2, B3, B4, B5 and B6, obtained at 3 different dwelling times), the characteristic pore size d_{84} and the product $[\varepsilon_a \cdot d_{84}^2]$. The characteristic diameter d_{84} represents the pore size above which remains the 84% in volume of the pores of the sample (measured from the total volume of intrusion) and is mainly related to finest pores of the pore size distribution. This volume of fine pores

poorly contributes to the enhancement of water permeability. Although both plots are straight lines, the simpler correlation based on pore size fits better the experimental data, owing to the great variety of the samples tested in which the starting composition (starch) and sintering conditions (sintering time) have simultaneously been changed. On the other hand, Hagen-Poiseuille equation assumes that tortuosity factor essentially keep constant for all the samples; however, this fact is not expected to be met in this type of ceramic pieces, as reported below. This finding is consistent with results obtained by the authors in previous works, which also showed the relationship between characteristic diameters and water permeability in low-cost ceramic membrane of different pore sizes [23,38,40].

3.4 Tortuosity estimate from a proposed model

As stated above, the Hagen-Poiseuille equation is normally used to predict the water permeability of membranes from membrane porosity and pore size [54]. However, this equation also introduces the tortuosity factor (τ). The tortuosity factor is defined as the ratio of the actual distance Δl travelled by the permeating species per unit length Δx of the filtrating medium. Since there are no experimental methods to directly evaluate the tortuosity, it is normally estimated by theoretical equations or empiric models [55]. In this section, the tortuosity factor has been calculated by a simple model, based on the Hagen-Poiseuille equation [Eq. 3] and the pore size distributions determined by mercury intrusion, showed in equation 4. This model has been successfully employed in previous works with low-cost ceramic membranes [23,40,56,57].

$$\boldsymbol{\tau} = \sqrt{\frac{\sum_{i=1}^{m}\left[\frac{a_i}{2}\left(r_{i_{max}}^4 - r_{i_{min}}^4\right) + \frac{b_i}{3}\left(r_{i_{max}}^3 - r_{i_{min}}^3\right)\right]}{8 \cdot \mu \cdot e^2 \cdot slp}} \qquad \textit{Eq. 4}$$

Where a_i and b_i are constants calculated from every interval i of the pore size distribution, r_{imax} and r_{imin} represent the maximum and minimum pore radius of every interval, μ is the water viscosity, e the membrane's thickness and slp the straight line's slope obtained in the water permeability test.

The data have been collected from previous sections and calculated tortuosity factors have been depicted in Figure 11. Comparing composition B0 (without starch) with the other compositions, it can be stated that the addition of a pore former significantly reduces the tortuosity factor; confirming previous reported works [23,40]. Moreover, overall the longer the dwelling time the lower the tortuosity factor is. Nevertheless, the nature of the starch added to the composition significantly influences the tortuosity factor as well as its variation with dwelling time. For example, composition B3 (higher sinterability, as set out above) shows the highest value of tortuosity factor at the shortest dwelling time (6 min) and the highest variation of this factor with dwelling time. Other compositions, such as B2, B4 and B5, exhibit a lower influence of dwelling time over tortuosity factor, as expected by their sintering behaviour. In general, these findings match well the sintering behaviour as well as the microstructure observations set out above. For this reason, it can be inferred that the ash content (and ash nature) of the starch affects the microstructure features of the ceramic membranes made up of starch as pore former, resulting in water permeability variations. There is also a correspondence between permeability and tortuosity factor, which represents the development of the ceramic membrane microstructure with sintering progress.

4 Conclusions

Starches are materials of natural origin which are provided by many sources. Because of this fact, they show a broad range of characteristics that influence their role as pore

former in low-cost ceramic membranes' compositions. Characteristics as water content, particle size distribution, ash content or composition of the ashes vary between wide margins, changing the properties of the ceramic membranes in which starches are used, mainly in sintered state.

In this investigation, starches of different sources and similar particle size were employed as pore formers for preparing low-cost ceramic membranes by uniaxial dry-pressing. The starting composition was based on a mixture of clay, calcite and chamotte, and different starches (6 samples) were added in the same proportion. Three dwelling times at the temperature of 1160ºC were tested.

The amount of ash left by the different starches ranged from 0.17 to 0.71 wt%. Besides, the analysis of these ashes revealed that they have different chemical composition, but a group of fluxing elements such as alkaline (sodium and potassium) and alkaline-earth (calcium) were main components in most of the samples. In general, it was observed that there is a certain direct relationship between sinterability (variation of open porosity and pore size with sintering time) and the total amount of fluxing elements present in the ashes. Nevertheless, owed to the complexity of the composition of the ashes, it is complicated to establish clear and simple correlations between some characteristics of the starches (chemical composition) and ceramic membrane's properties or sintering behaviour.

Finally, by means of a simple model, the tortuosity factor was calculated and it was stated that its value, as well as the influence of dwelling time over it, changed depending on the nature of the starch.

It is worth mentioning that the membranes developed in this work will be employed as supports of multilayer ceramic membranes for ultra and nanofiltration by developing thinner, selective layers, which will be addressed in future research.

Acknowledgements

This material is based upon work supported by the Spanish Ministry of Science and Innovation through the National Plan for Scientific Research, Development and Technology Innovation 2008-2011 (INNPACTO programme, project IPT-2011-1069-310000).

The authors wish to thank the personnel of FACSA (José Guillermo Berlanga, Ernesto Santateresa and Anna Gozalbo) and University of Zaragoza (Miguel Menendez, Joaquín Coronas, Raquel Alcalá and Olga Pérez) for their helpful aid during the execution of the present work.

References

[1] J.M. Benito, A. Conesa, M.A. Rodríguez, Membranas cerámicas. Tipos, métodos de obtención y caracterización, Bol. Soc. Esp. Ceram. V. 43 (2004) 829–842.

[2] R.W. Baker, Membrane technology and applications, 2nd ed., Wiley, Chichester, 2004.

[3] R. Mallada, M. Menéndez, Inorganic membranes synthesis, characterization and applications, 1st ed., Elsevier B.V., Oxford, 2008.

[4] A.J. Burggraaf, L. Cot, Fundamentals of Inorganic Membranes, Science and Technology, Elsevier, Amsterdam, 1996.

[5] M. Mulder, Basic Principes of Membrane Technology, 2nd ed., Kluwer Academic Publishers, Dordrecht, The Netherlands, 1996.

[6] S. Emani, R. Uppaluri, M.K. Purkait, Preparation and characterization of low cost ceramic membranes for mosambi juice clarification, Desalination. 317 (2013)

32–40. doi:10.1016/j.desal.2013.02.024.

[7] E. Drioli, L. Giorno, Comprehensive membrane science and engineering. Vol 1: Basic aspects of membrane science and engineering, Elsevier, Kidlington, 2010.

[8] P. Belibi Belibi, M.M.G. Nguemtchouin, M. Rivallin, J. Ndi Nsami, J. Sieliechi, S. Cerneaux, M.B. Ngassoum, M. Cretin, Microfiltration ceramic membranes from local Cameroonian clay applicable to water treatment, Ceram. Int. 41 (2015) 2752–2759. doi:10.1016/j.ceramint.2014.10.090.

[9] M. Almandoz, C.L. Pagliero, N.A. Ochoa, J. Marchese, Composite ceramic membranes from natural aluminosilicates for microfiltration applications, Ceram. Int. 41 (2015) 5621–5633. doi:10.1016/j.ceramint.2014.12.144.

[10] I. Hedfi, N. Hamdi, E. Srasra, M.A. Rodríguez, The preparation of micro-porous membrane from a Tunisian kaolin, Appl. Clay Sci. 101 (2014) 574–578. doi:10.1016/j.clay.2014.09.021.

[11] A. Harabi, F. Zenikheri, B. Boudaira, F. Bouzerara, A. Guechi, L. Foughali, A new and economic approach to fabricate resistant porous membrane supports using kaolin and CaCO3, J. Eur. Ceram. Soc. 34 (2014) 1329–1340. doi:10.1016/j.jeurceramsoc.2013.11.007.

[12] A. Majouli, S. Tahiri, S. Alami Younssi, H. Loukili, A. Albizane, Elaboration of new tubular ceramic membrane from local Moroccan Perlite for microfiltration process. Application to treatment of industrial wastewaters, Ceram. Int. 38 (2012) 4295–4303. doi:10.1016/j.ceramint.2012.02.010.

[13] D. Vasanth, G. Pugazhenthi, R. Uppaluri, Fabrication and properties of low cost ceramic microfiltration membranes for separation of oil and bacteria from its solution, J. Memb. Sci. 379 (2011) 154–163. doi:10.1016/j.memsci.2011.05.050.

[14] S. Khemakhem, A. Larbot, R. Ben Amar, New ceramic microfiltration membranes from Tunisian natural materials: Application for the cuttlefish effluents treatment, Ceram. Int. 35 (2009) 55–61. doi:10.1016/j.ceramint.2007.09.117.

[15] F. Bouzerara, A. Harabi, S. Achour, A. Larbot, Porous ceramic supports for membranes prepared from kaolin and doloma mixtures, J. Eur. Ceram. Soc. 26 (2006) 1663–1671. doi:10.1016/j.jeurceramsoc.2005.03.244.

[16] S. Bose, C. Das, Sawdust: From wood waste to pore-former in the fabrication of ceramic membrane, Ceram. Int. 41 (2015) 4070–4079. doi:10.1016/j.ceramint.2014.11.101.

[17] J. Cao, X. Dong, L. Li, Y. Dong, S. Hampshire, Recycling of waste fly ash for production of porous mullite ceramic membrane supports with increased porosity, J. Eur. Ceram. Soc. 34 (2014) 3181–3194. doi:10.1016/j.jeurceramsoc.2014.04.011.

[18] I. Jedidi, S. Khemakhem, L. Messouadi, A. Larbot, M. Rafiq, L. Cot, R. Ben Amar, Elaboration and characterisation of fly ash based mineral supports for microfiltration and ultrafiltration membranes, Ceram. Int. 35 (2009) 2747–2753. doi:10.1016/j.ceramint.2009.03.021.

[19] S. Vijayan, R. Narasimman, K. Prabhakaran, A urea crystal templating method for the preparation of porous alumina ceramics with the aligned pores, J. Eur. Ceram. Soc. 33 (2013) 1929–1934. doi:10.1016/j.jeurceramsoc.2013.02.031.

[20] G.C.C. Yang, C.-M. Tsai, Effects of starch addition on characteristics of tubular porous ceramic membrane substrates, Desalination. 233 (2008) 129–136. doi:10.1016/j.desal.2007.09.035.

[21] E. Sánchez, S. Mestre, V. Pérez-Herranz, M. García-Gabaldón, Síntesis de membranas cerámicas para la regeneración de baños de cromado agotados, Bol. Soc. Esp. Ceram. V. 44 (2005) 409–414.

[22] E. Gregorová, W. Pabst, I. Bohačenko, Characterization of different starch types for their application in ceramic processing, J. Eur. Ceram. Soc. 26 (2006) 1301–1309. doi:10.1016/j.jeurceramsoc.2005.02.015.

[23] M.-M. Lorente-Ayza, E. Sánchez, V. Sanz, S. Mestre, Influence of starch content on the properties of low-cost microfiltration ceramic membranes, Ceram. Int. (2015). doi:10.1016/j.ceramint.2015.07.092.

[24] F.A. Almeida, E.C. Botelho, F.C.L. Melo, T.M.B. Campos, G.P. Thim, Influence of cassava starch content and sintering temperature on the alumina consolidation technique, J. Eur. Ceram. Soc. 29 (2009) 1587–1594. doi:10.1016/j.jeurceramsoc.2008.10.006.

[25] S. Li, C.-A. Wang, J. Zhou, Effect of starch addition on microstructure and properties of highly porous alumina ceramics, Ceram. Int. 39 (2013) 8833–8839. doi:10.1016/j.ceramint.2013.04.072.

[26] F. Bouzerara, A. Harabi, S. Condom, Porous ceramic membranes prepared from kaolin, Desalin. Water Treat. 12 (2009) 415–419. doi:10.5004/dwt.2009.1051.

[27] M.M. Bazin, M.A. Ahmat, N. Zaidan, A.F. Ismail, N. Ahmad, Effect of starch addition on microstructure and strength of ball clay membrane, J. Teknol. (Sciences Eng. 69 (2014) 117–120.

[28] G.P. Jiang, J.F. Yang, J.Q. Gao, Effect of starch on extrusion behaviour of ceramic pastes, Mater. Res. Innov. 13 (2009) 119–123. doi:10.1179/143307509X435664.

[29] E. Gregorová, W. Pabst, Z. Živcová, I. Sedlářová, S. Holíková, Porous alumina ceramics prepared with wheat flour, J. Eur. Ceram. Soc. 30 (2010) 2871–2880. doi:10.1016/j.jeurceramsoc.2010.03.020.

[30] E. Gregorová, W. Pabst, Porous ceramics prepared using poppy seed as a pore-forming agent, Ceram. Int. 33 (2007) 1385–1388. doi:10.1016/j.ceramint.2006.05.019.

[31] S. Bose, C. Das, Preparation and characterization of low cost tubular ceramic support membranes using sawdust as a pore-former, Mater. Lett. 110 (2013) 152–155. doi:10.1016/j.matlet.2013.08.019.

[32] J.K. Efavi, L. Damoah, D.Y. Bensah, D.D. Arhin, D. Tetteh, Development of porous ceramic bodies from kaolin deposits for industrial applications, Appl. Clay Sci. 65-66 (2012) 31–36. doi:10.1016/j.clay.2012.04.010.

[33] E. Chevalier, D. Chulia, C. Pouget, M. Viana, Fabrication of porous substrates: a review of processes using pore forming agents in the biomaterial field, J. Pharm. Sci. 97 (2008) 1135–1154.

[34] M.H. Talou, M.A. Camerucci, Two alternative routes for starch consolidation of mullite green bodies, J. Eur. Ceram. Soc. 30 (2010) 2881–2887. doi:10.1016/j.jeurceramsoc.2010.06.001.

[35] H.M. Alves, G. Tarì, A.T. Fonseca, J.M.F. Ferreira, Processing of porous cordierite bodies by starch consolidation, Mater. Res. Bull. 33 (1998) 1439–1448.

[36] O. Lyckfeldt, J.M.F. Ferreira, Processing of Porous Ceramics by “Starch Consolidation,” J. Eur. Ceram. Soc. 18 (1998) 131–140.

[37] E. Gregorová, W. Pabst, Porosity and pore size control in starch consolidation casting of oxide ceramics—Achievements and problems, J. Eur. Ceram. Soc. 27

(2007) 669–672. doi:10.1016/j.jeurceramsoc.2006.04.048.

[38] M.-M. Lorente-Ayza, M.J. Orts, V. Pérez-Herranz, S. Mestre, Role of starch characteristics in the properties of low-cost ceramic membranes, J. Eur. Ceram. Soc. 35 (2015) 2333–2341. doi:10.1016/j.jeurceramsoc.2015.02.026.

[39] A. Diaz, S. Hampshire, Characterisation of porous silicon nitride materials produced with starch, J. Eur. Ceram. Soc. 24 (2004) 413–419. doi:10.1016/S0955-2219(03)00212-7.

[40] M.-M. Lorente-Ayza, S. Mestre, M. Menéndez, E. Sánchez, Comparison of extruded and pressed low cost ceramic supports for microfiltration membranes, J. Eur. Ceram. Soc. 35 (2015) 3681–3691. doi:10.1016/j.jeurceramsoc.2015.06.010.

[41] J.L. Amorós, V. Beltrán, A. Blasco, C. Feliu, M. Sancho-Tello, Técnicas experimentales del control de la compactación de pavimentos y revestimientos cerámicos, Técnica Cerámica. 116 (1983) 1234–1246.

[42] A. Barba, V. Beltrán, C. Feliu, J. García-Ten, F. Ginés, E. Sánchez, V. Sanz, Materias primas para la fabricación de soportes de baldosas cerámicas, 2nd ed., Instituto de Tecnología Cerámica, Castellón, 2000.

[43] H. Giesche, Mercury Porosimetry: A General (Practical) Overview, Part. Part. Syst. Charact. 23 (2006) 9–19. doi:10.1002/ppsc.200601009.

[44] P. Maarten Biesheuvel, H. Verweij, Design of ceramic membrane supports: permeability, tensile strength and stress, J. Memb. Sci. 156 (1999) 141–152. doi:10.1016/S0376-7388(98)00335-4.

[45] H. Strathmann, L. Giorno, E. Drioli, An introduction to membrane science and technology, Consiglio Nazionale delle Ricerche, Roma, 2006.

[46] R. Pérez-Gálvez, E.M. Guadix, J.P. Bergé, A. Guadix, Operation and cleaning of

ceramic membranes for the filtration of fish press liquor, J. Memb. Sci. 384 (2011) 142–148. doi:10.1016/j.memsci.2011.09.019.

[47] S. Sales, M.-M. Lorente-Ayza, J. Gilabert, E. Sánchez, S. Mestre, Efecto de las características del almidón sobre la permeabilidad de las membranas cerámicas, in: XIII Congr. Nac. Mater., Barcelona, 2014: p. 115.

[48] M.-M. Lorente-Ayza, M.J. Orts, V. Pérez-Herranz, S. Mestre, Role of starch characteristics in the densification of ceramic membranes based on traditional raw materials, in: 14th Int. Conf. Eur. Ceram. Soc., Toledo (Spain), 2015.

[49] Y. Chen, A. Burbidge, J. Bridgwater, Effect of carbohydrate on the rheological parameters of paste extrusion, J. Am. Ceram. Soc. 80 (1997) 1841–1850.

[50] S.J. Kang, Sintering. Densification, grain growth & microstructure, Elsevier Ltd, Oxford, 2005.

[51] M.N. Rahaman, Ceramic processing and sintering, 2nd ed., Marcel Dekker, INC., New York, 2003.

[52] J.L. Amorós, M.J. Orts, A. Escardino, A. Blasco, Evolution of pore-size distribution during the firing of stoneware floor tile, in: Qualicer'96 "IV Congr. Mund. La Calid. Del Azulejo Y Del Paviment. Cerámico," Castellón, 1996: pp. 737–740.

[53] M.J. Orts, Sinterización de piezas de pavimento gresificado, Universitat de Valencia, 1991.

[54] W. Li, W. Xing, N. Xu, Modeling of relationship between water permeability and microstructure parameters of ceramic membranes, Desalination. 192 (2006) 340–345. doi:10.1016/j.desal.2005.07.042.

[55] L. Shen, Z. Chen, Critical review of the impact of tortuosity on diffusion, Chem.

Eng. Sci. 62 (2007) 3748–3755. doi:10.1016/j.ces.2007.03.041.

[56] S. Sales, Intercambiadores iónicos inorgánicos nanoestructurados: síntesis e infiltración en membranas cerámicas. PhD thesis, Universitat Jaume I, 2015.

[57] J. Gilabert, Relación del coeficiente de permeabilidad de membranas cerámicas con las condiciones de síntesis. MsC thesis, Universitat Jaume I, 2012.

Figure Captions

Figure 1. Particle size distribution of the inorganic raw materials used in this work after dry-milling.

Figure 2. Thermal cycle for the different membrane samples with a dwell time at maximum sintering temperature of 6, 60 or 120 min.

Figure 3. Starches' particle size distribution.

Figure 4. Water uptake of compositions at different dwelling times (T=1160ºC).

Figure 5. Relation between water uptake difference and fluxing content in the ashes.

Figure 6. Pore size distribution of the ceramic membranes obtained from the 3 dwelling times (6, 60 and 120 minutes): composition B2 (a) and composition B3 (b).

Figure 7. Evolution of the mean pore size d_{50} of the ceramic membranes obtained from the six compositions with dwelling time.

Figure 8. FEG-ESEM micrographs of supports sintered at 6 or 120 min of dwell time at maximum sintering temperature (Magnification: 400x). Samples: B2, B3 and B4.

Figure 9. Variation of water permeability with dwelling time for all membrane compositions.

Figure 10. Plot of water permeability values (K_p) of all the supports (B1, B2, B3, B4, B5 and B6, at 3 different dwelling times) versus d_{84} and ($\varepsilon_{sf} \cdot d_{84}^2$).

Figure 11. Variation of tortuosity with dwelling time (T=1160ºC).

Table 1. Source and provider of the starches used in this work.

Reference	Source	Provider
M1	Corn	Roquette Freres S.A., France
M2	Potato	Sigma-Aldrich Co. USA
M3	Potato	Roquette Freres S.A., France
M4	Wheat	Fisher Chemical, USA
M5	Wheat	Roquette Freres S.A., France
M6	Pea	Roquette Freres S.A., France

Table 2. Chemical and mineralogical compositions of the raw materials used (wt %).

	Clay mixture	Calcite	Chamotte
SiO_2	67.2	0.24	70.1
Al_2O_3	20.3	0.15	20.4
Fe_2O_3	1.1	0.02	1.7
CaO	0.4	55.7	0.5
MgO	0.5	0.14	0.4
Na_2O	0.2	-	4.3
K_2O	3.0	0.01	2.0
TiO_2	1.0	-	0.7
Loss on ignition	6.3	43.7	-
Mineralogical composition	Kaolinite, Quartz; Albite, Microcline (potassium feldspar) Muscovite, Hematite	Calcite	Quartz, Albite, Microcline, Hematite

Table 03

Table 3. Ceramic membrane compositions prepared in this work (wt %).

Composition	B0	B1	B2	B3	B4	B5	B6
Clay	60	40	40	40	40	40	40
Chamotte	20	20	20	20	20	20	20
Calcite	20	20	20	20	20	20	20
M1	-	20	-	-	-	-	-
M2	-	-	20	-	-	-	-
M3	-	-	-	20	-	-	-
M4	-	-	-	-	20	-	-
M5	-	-	-	-	-	20	-
M6	-	-	-	-	-	-	20

Table 4. Starches' particle size parameters obtained from particle size distribution curves.

Sample	D_{10} (μm)	D_{50} (μm)	D_{90} (μm)	D_{90} - D_{10} (μm)
M1	9	14	22	13
M2	22	39	67	45
M3	26	46	76	50
M4	9	14	23	14
M5	12	20	31	19
M6	17	24	33	16

Table 5. Water content of as-received starch samples and ash content after samples' burnout.

Starch	Water content (%)[1]	Ash content (%)[2]
M1	14.6	0.32
M2	16.8	0.17
M3	22.3	0.71
M4	9.9	0.49
M5	14.7	0.37
M6	14.6	0.29

[1] As received

[2] After thermal treatment

Table 6. Chemical composition in terms of identified elements of the ashes (denoted by A) of the studied starches (wt%). Note that A1 to A6 refers to ashes obtained from M1 to M6 starch samples.

Element (wt%)	A1	A2	A3	A4	A5	A6
Na	10	5.1	0.9	2.2	14	26
Mg	2.5	2.0	1.7	1.1	0.8	1.3
Al	0.3	0.2	-	<0.1	-	0.2
Si	0.9	0.8	0.3	0.4	0.3	0.9
P	24	23	20	20	20	8.3
S	-	-	-	-	-	0.8
K	12	22	6.8	24	7.6	16
Ca	3.2	3.4	14	2.1	4.0	2.1
Cu	2.0	1.4	1.7	1.5	4.1	0.5
Zn	1.6	1.2	1.3	1.1	2.8	0.5
Calculated total amount (wt%) of Na, K and Ca in the ash $[(Na+K+Ca)_A]$ [3]	0.08	0.05	0.16	0.14	0.10	0.13

[3] This amount has been calculated from ash content of Table 5.

Table 7. Bulk density values of unfired support specimens.

Composition	B0	B1	B2	B3	B4	B5	B6
Dry bulk density (g/cm^3)	1.91 ± 0.01	1.52 ± 0.01	1.56 ± 0.01	1.56 ± 0.01	1.54 ± 0.01	1.54 ± 0.01	1.55 ± 0.01

Table 8. Sintering parameters of the six ceramic membrane compositions studied at soaking time of 60 minutes (T=1160ºC).

Composition	B0	B1	B2	B3	B4	B5	B6
Linear Shrinkage (%)	0.5±0.1	2.8±0.3	1.6±0.2	1.9±0.1	0.8±0.1	2.8±0.1	2.0±0.1
Water uptake (%)	19.9±0.2	45.2±0.1	46.4±0.6	44.1±0.5	49.4±0.3	43.5±0.2	45.7±0.4
Loss on ignition (%)	13.41±0.02	30.32±0.02	29.78±0.02	29.29±0.02	29.52±0.01	30.17±0.01	30.17±0.02
Sintered bulk density (g/cm^3)	1.72±0.01	1.22±0.02	1.19±0.01	1.22±0.01	1.14±0.01	1.23±0.01	1.20±0.01
Open porosity ε_a (%)	34.2±0.1	55.1±0.2	55.0±0.4	53.8±0.2	56.5±0.2	53.4±0.1	54.6±0.1

Table 09

Table 9. Water permeability of the ceramic membranes obtained from the six compositions together with the mean particle size of the starch used.

Composition	Soaking time (min)	B0	B1	B2	B3	B4	B5	B6
K_p *10^{-14} (m^2)	6	12	100	110	80	70	120	100
	60	31	180	240	250	160	220	200
	120	-	290	250	390	330	290	290
P_e *10^2 ($L \cdot h^{-1} \cdot m^{-2} \cdot bar^{-1}$)	6	62	200	190	130	120	210	180
	60	160	360	450	460	280	420	390
	120	-	570	490	780	690	570	560
D_{50} (µm)	-	-	14	39	46	14	20	24

Figure 01
Click here to download high resolution image

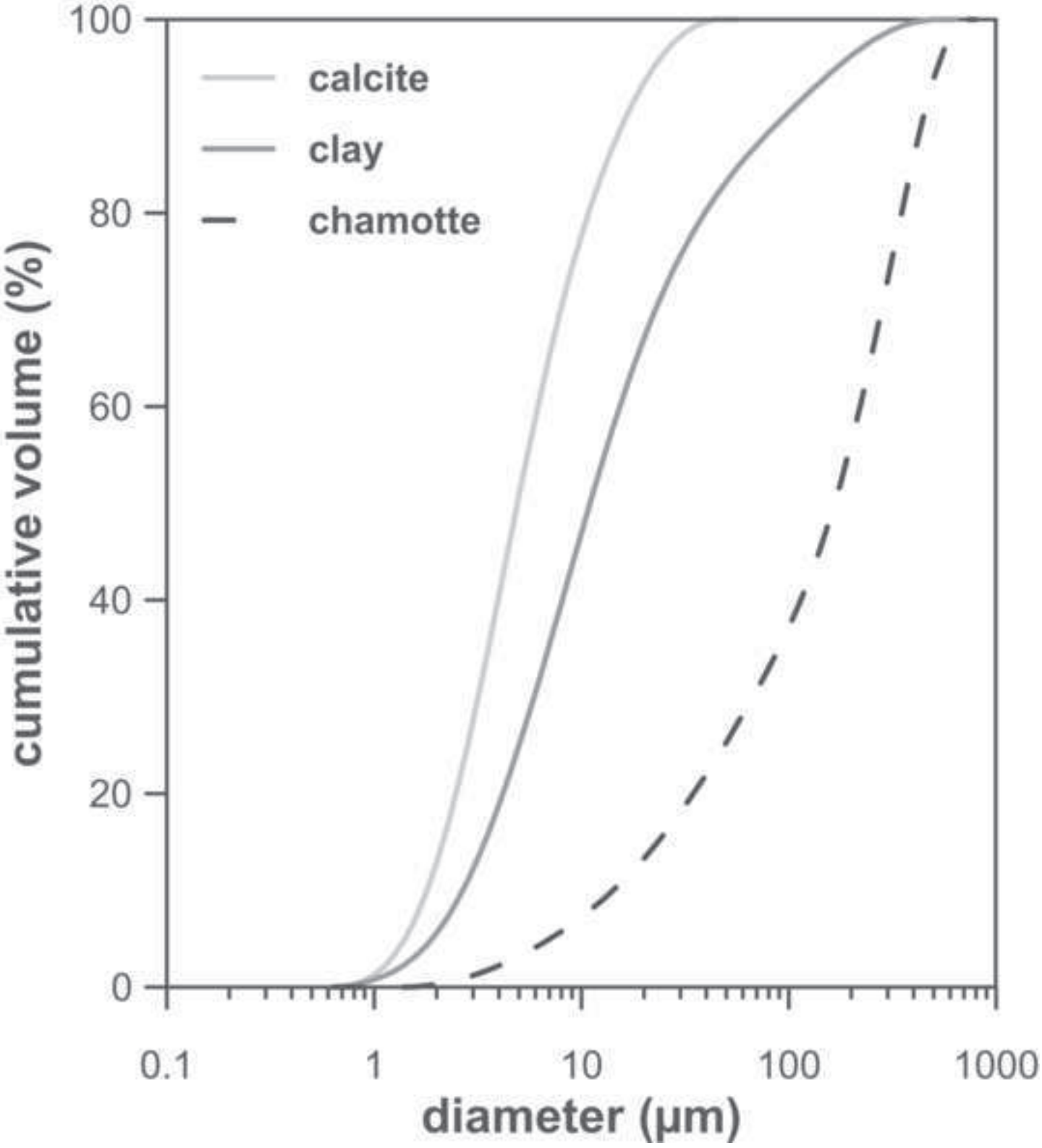

Figure 02
Click here to download high resolution image

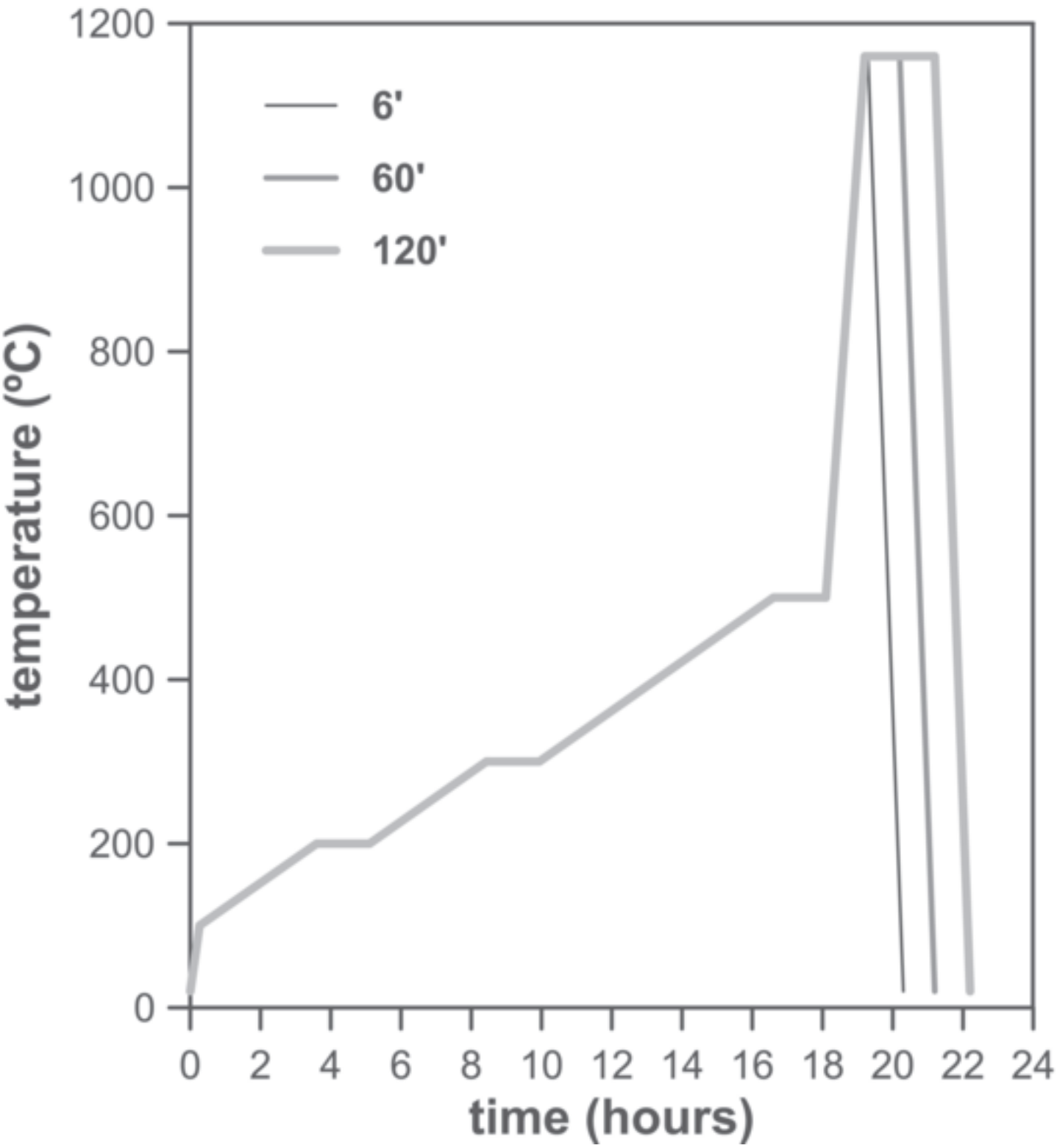

Figure 03
Click here to download high resolution image

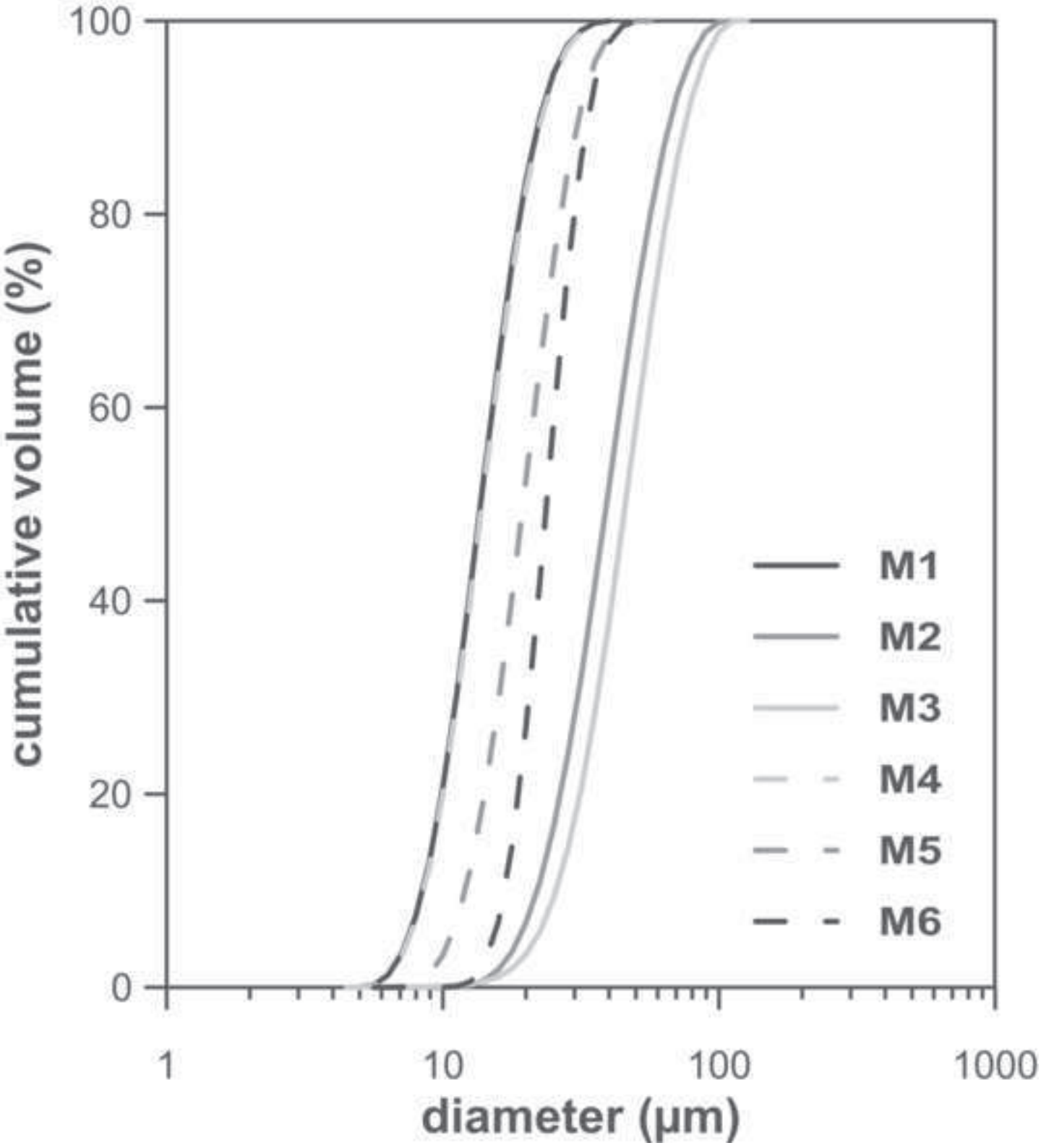

Figure 04
Click here to download high resolution image

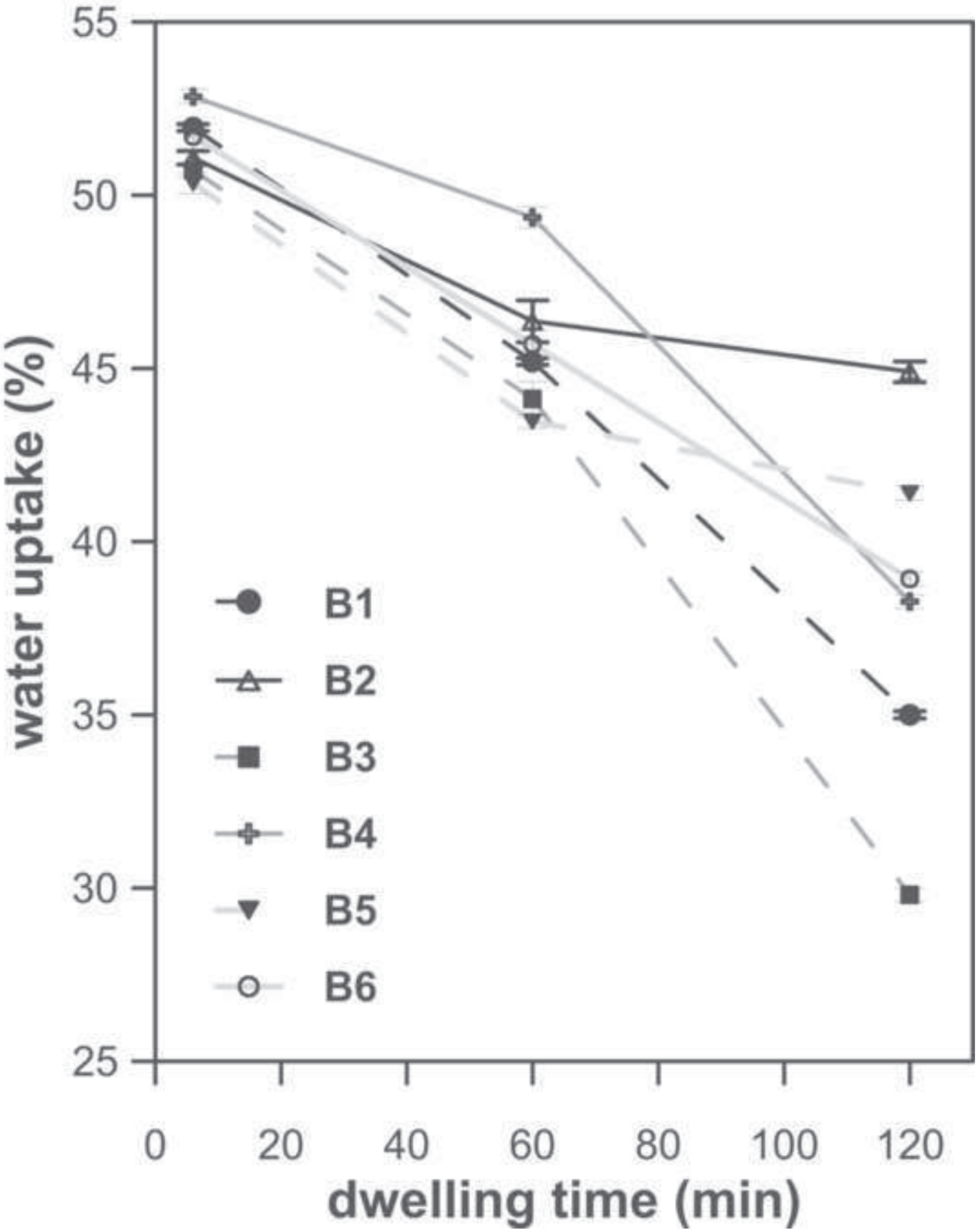

Figure 05
Click here to download high resolution image

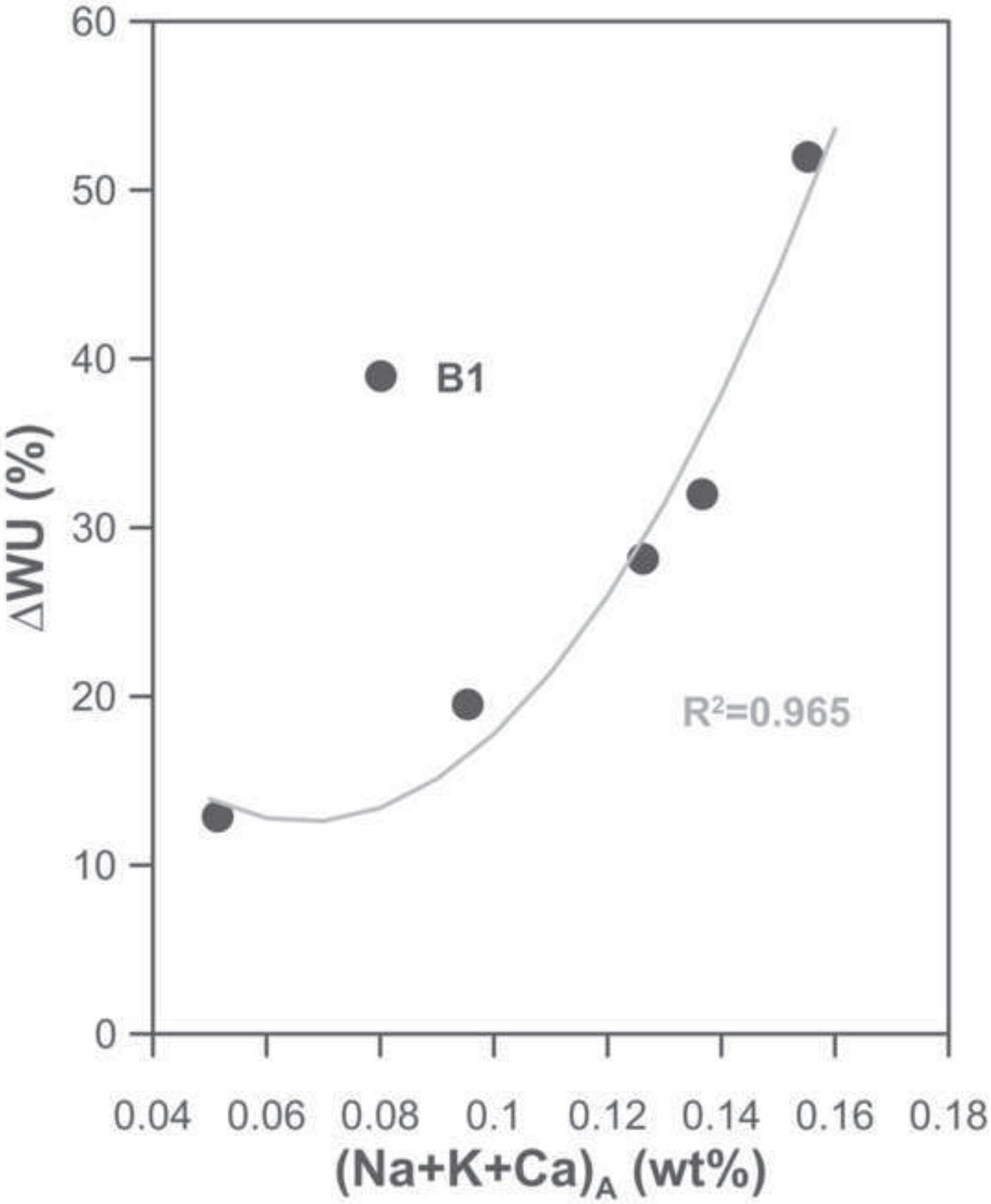

Figure 06

Click here to download high resolution image

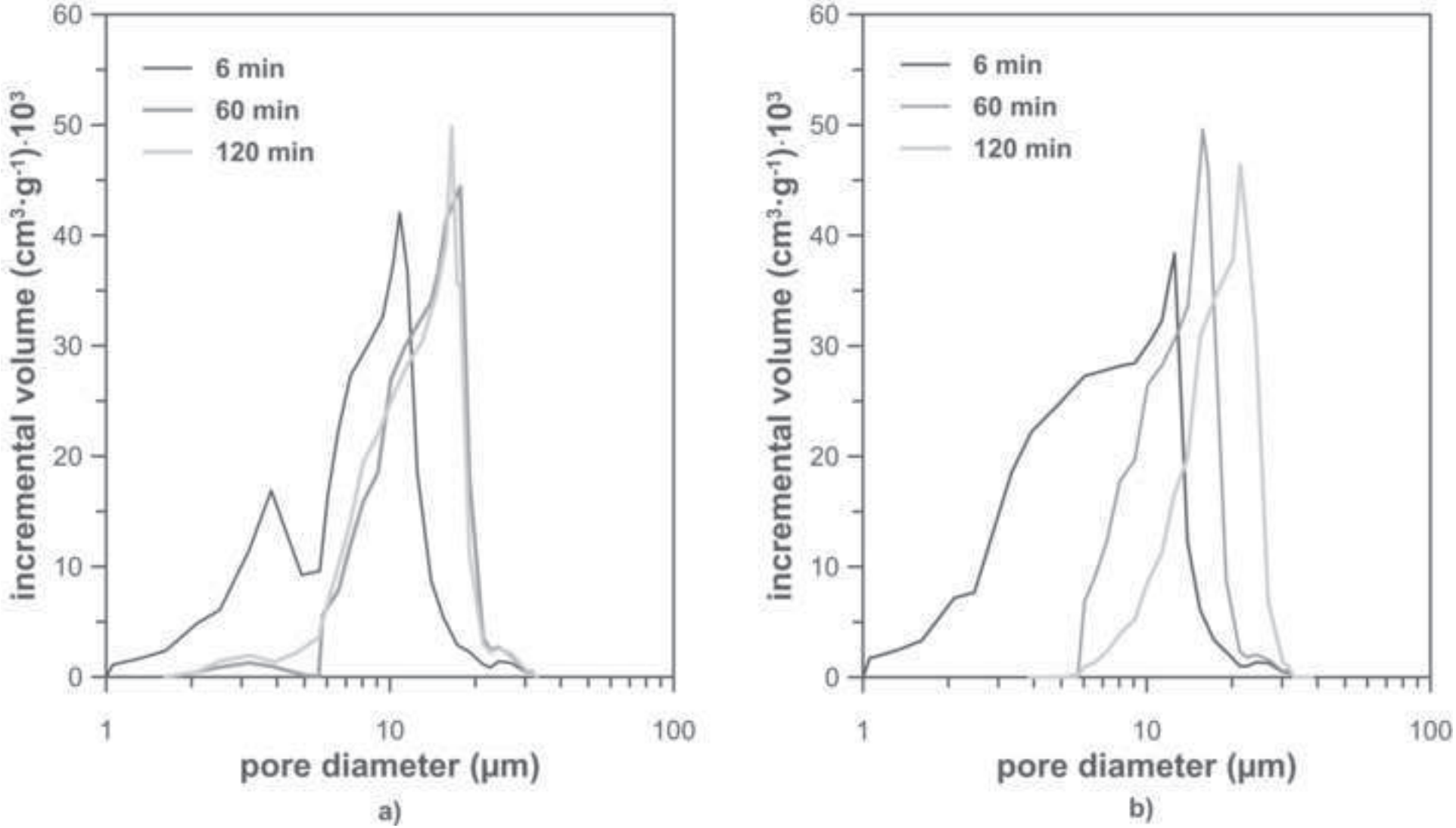

Figure 07
Click here to download high resolution image

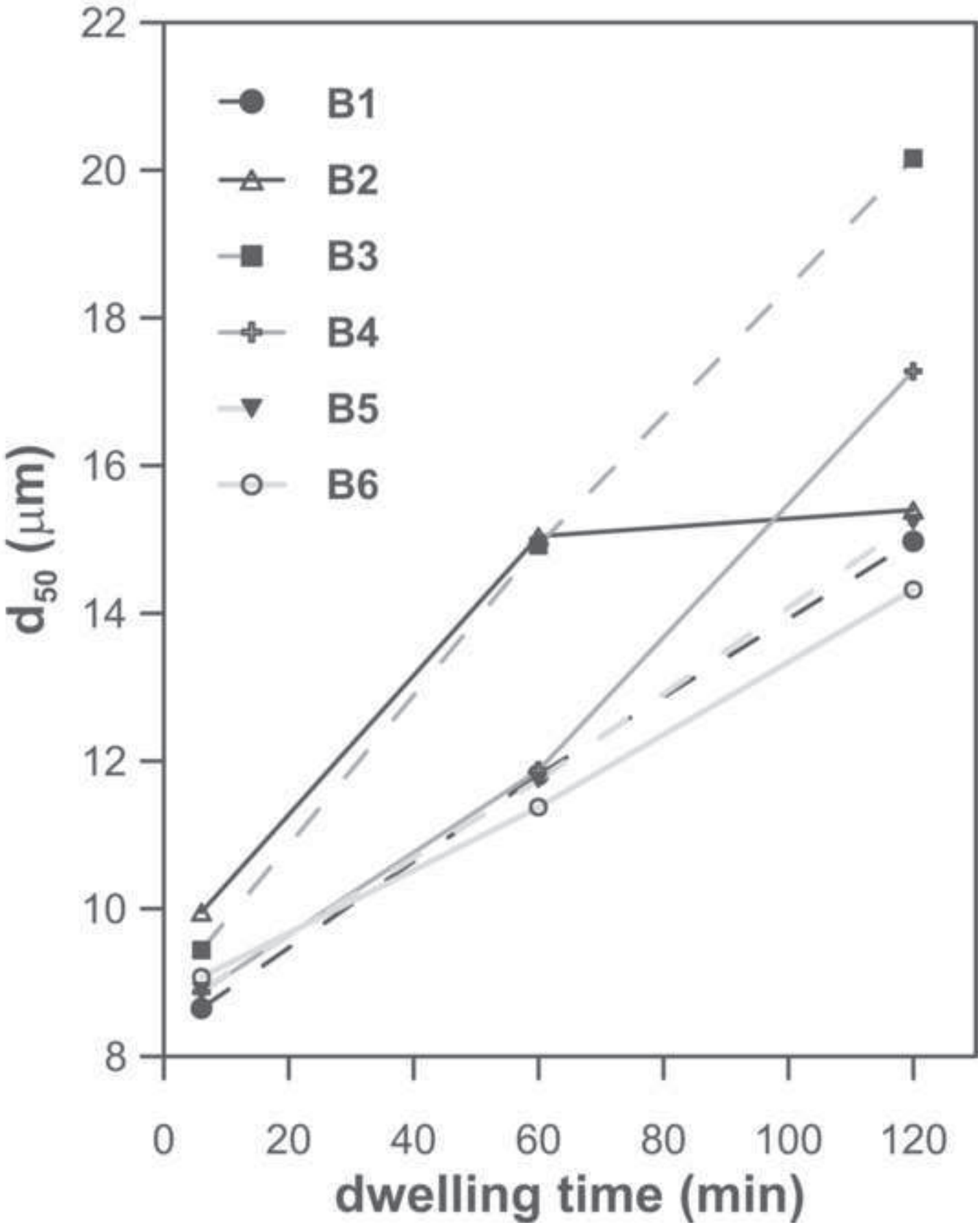

Figure 08
Click here to download high resolution image

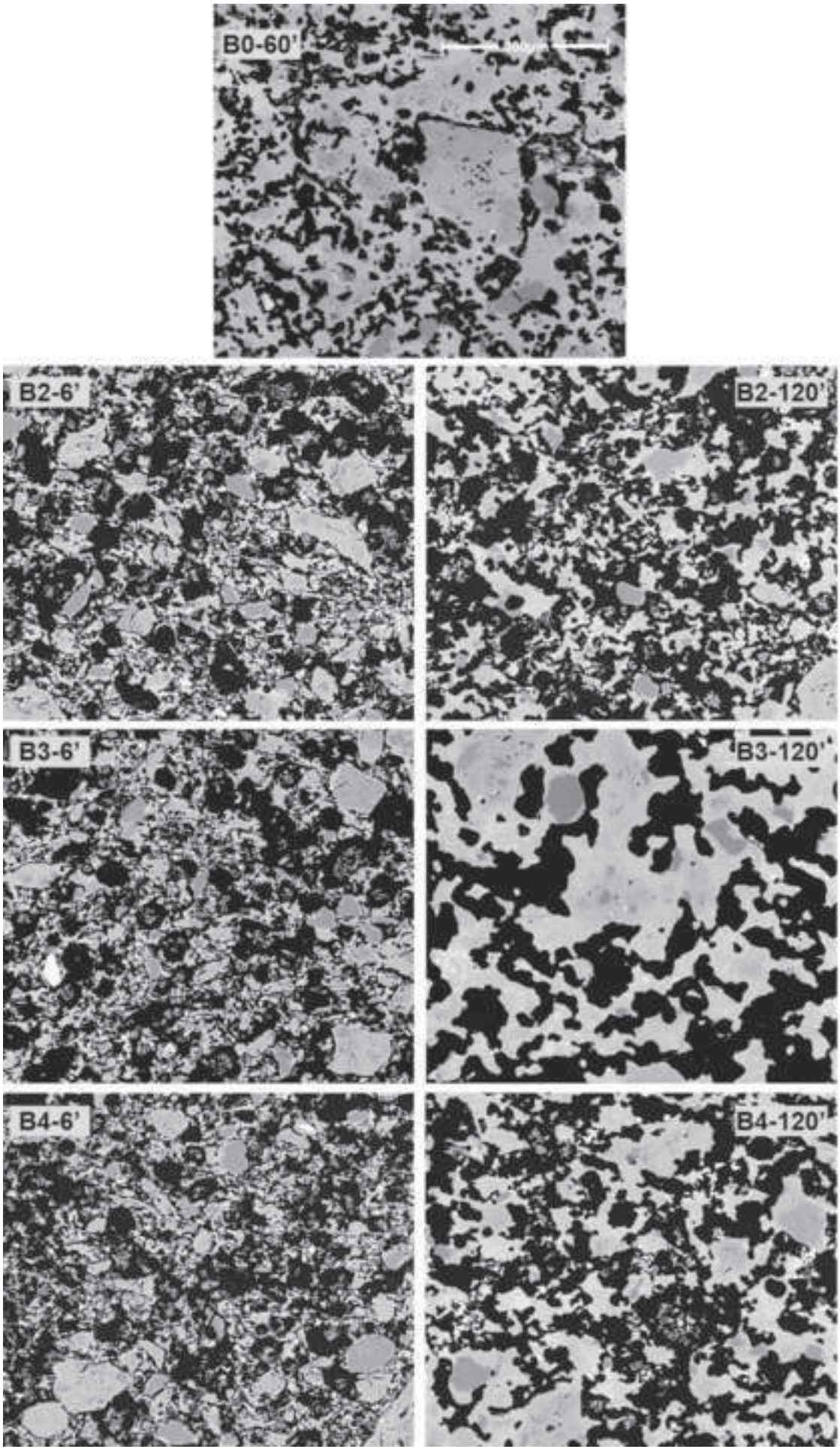

Figure 09
Click here to download high resolution image

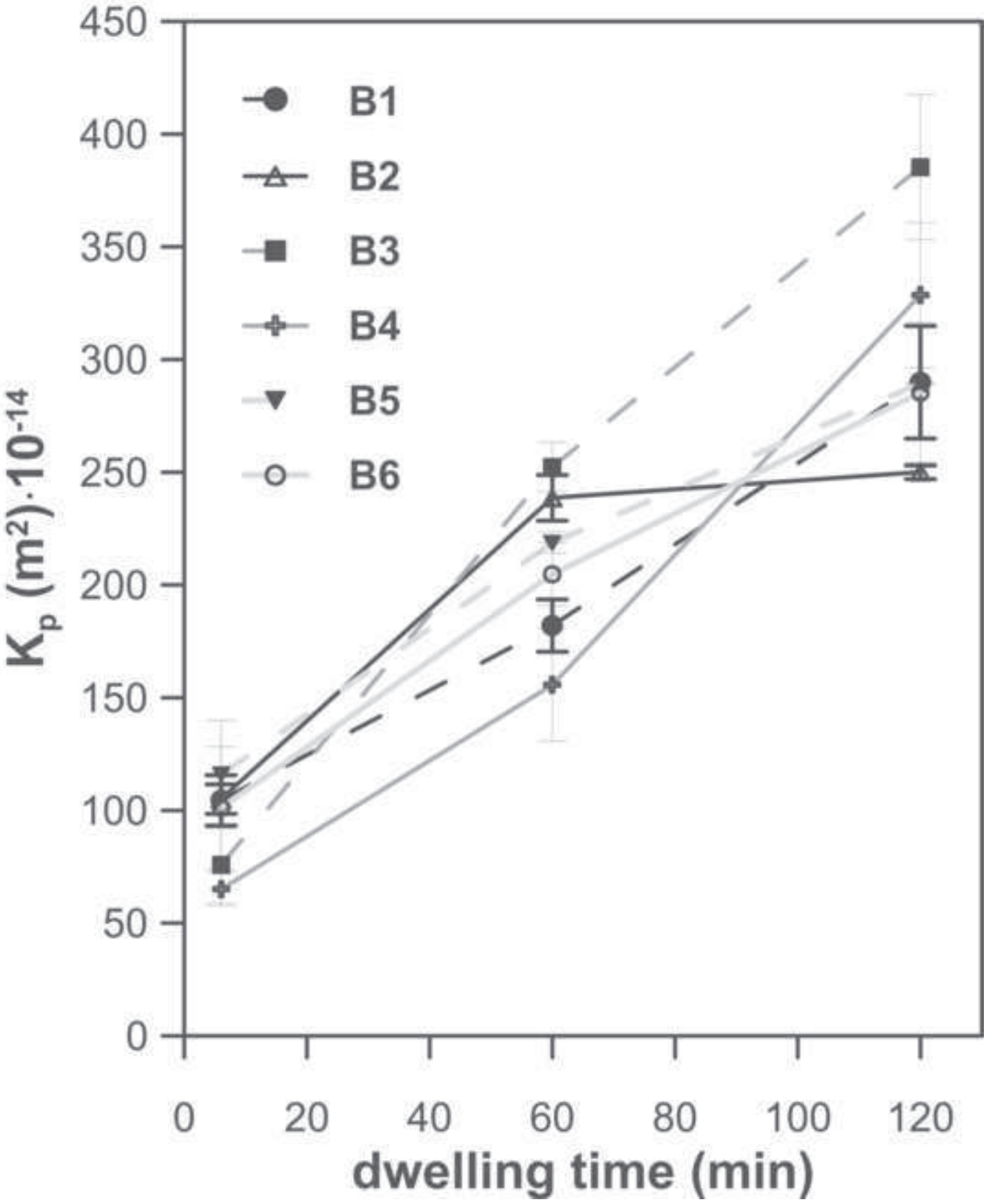

Figure 10
Click here to download high resolution image

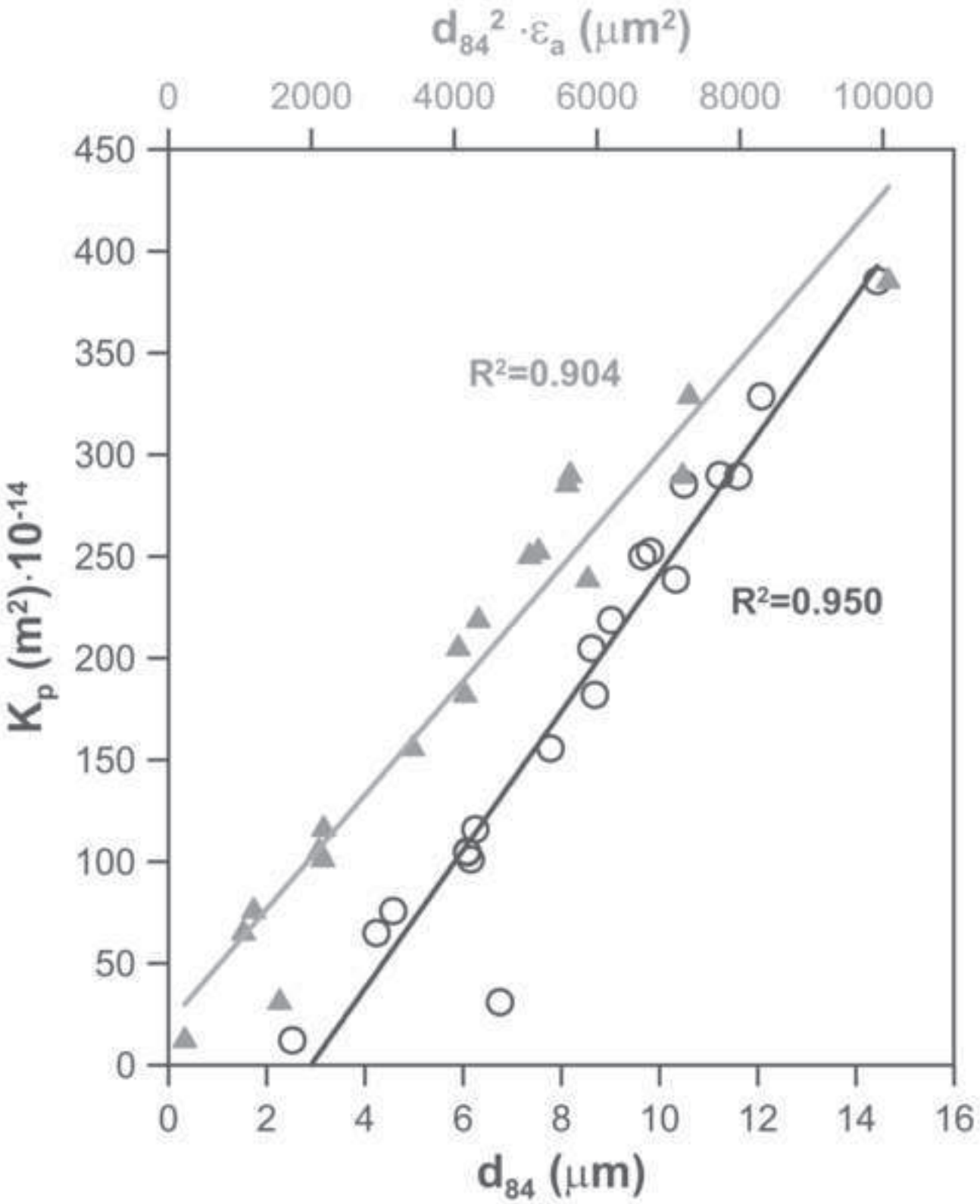
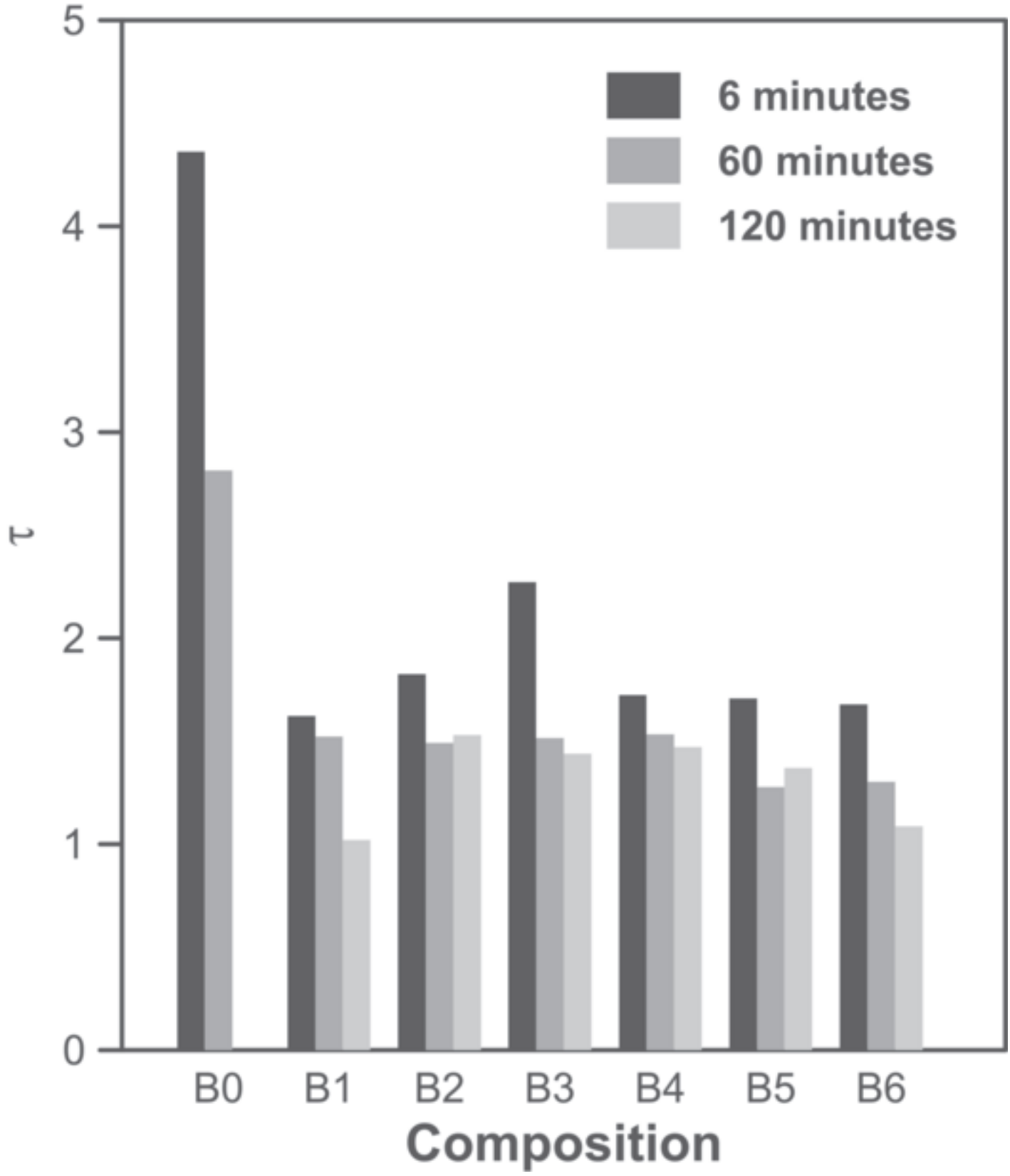
Figure 11
Click here to download high resolution image